Supplement of Atmos. Chem. Phys., 23, 15235–15252, 2023
https://doi.org/10.5194/acp-23-15235-2023-supplement

Atmospheric Chemistry and Physics Open Access

Supplement of

Decreasing trends of ammonia emissions over Europe seen from remote sensing and inverse modelling

Ondřej Tichý et al.

Correspondence to: Nikolaos Evangeliou (nikolaos.evangeliou@nilu.no)

SUPPLEMENTARY FIGURES

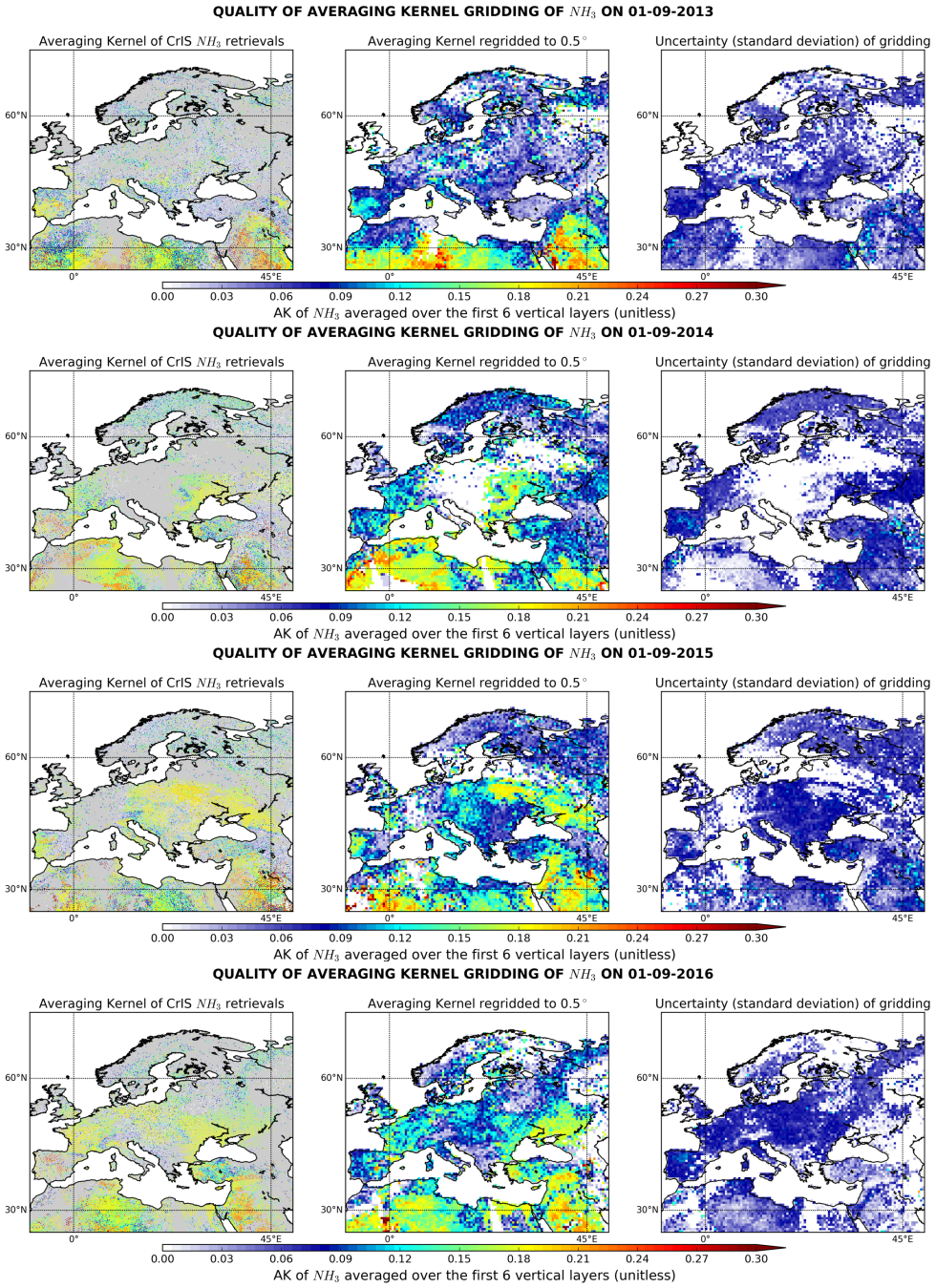

Supplementary Figure S 1. Quality and evaluation of daily gridded averaging kernel values of CrIS ammonia in the first six vertical levels. As an example, daily observations of the kernel values (left panel), daily 0.5°×0.5° gridded kernels (middle panel) and their gridded standard deviation are plotted for 1st September of all years of the study period (2013–2020).

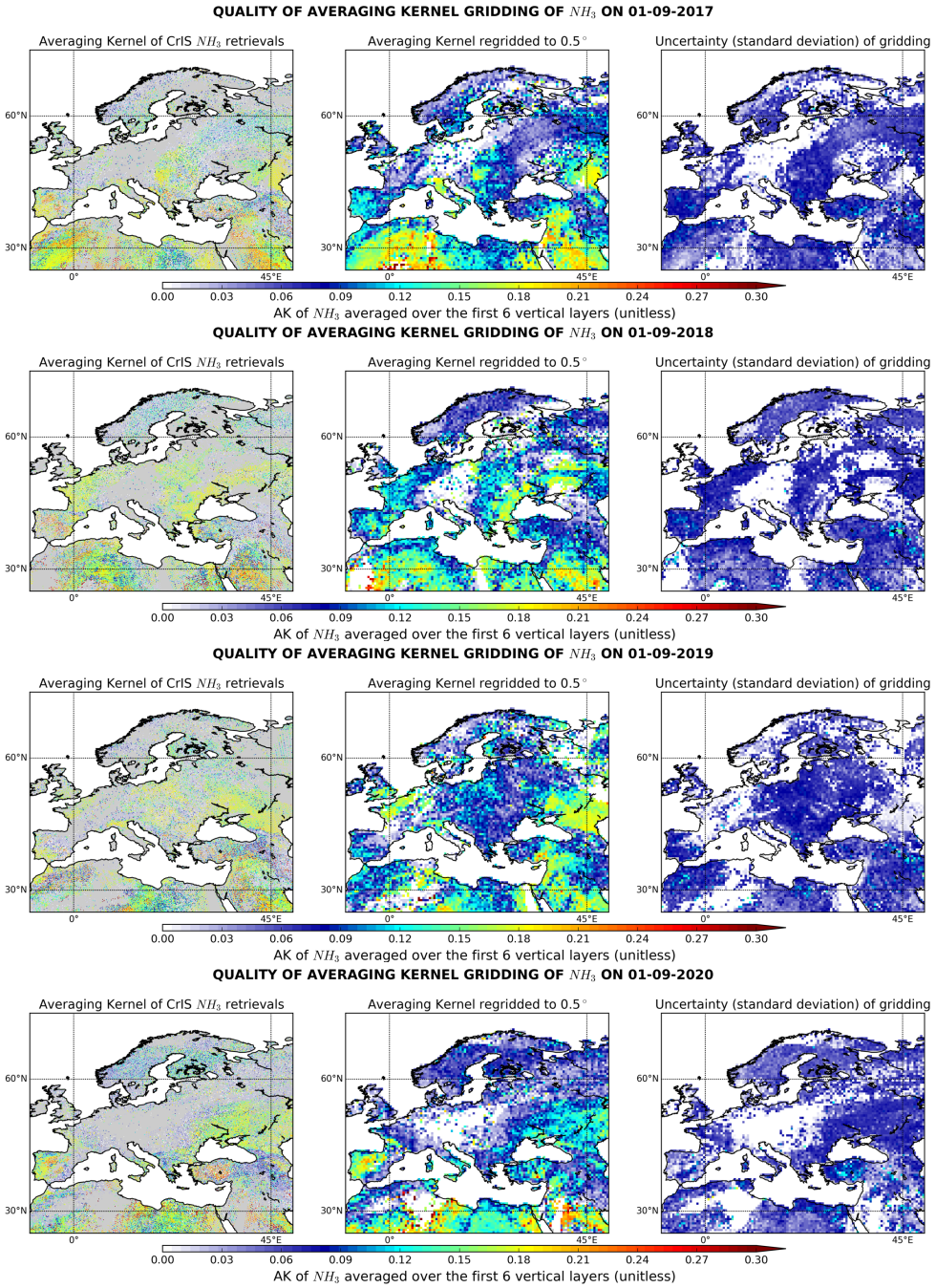

Supplementary Figure S 1. *Continued.*

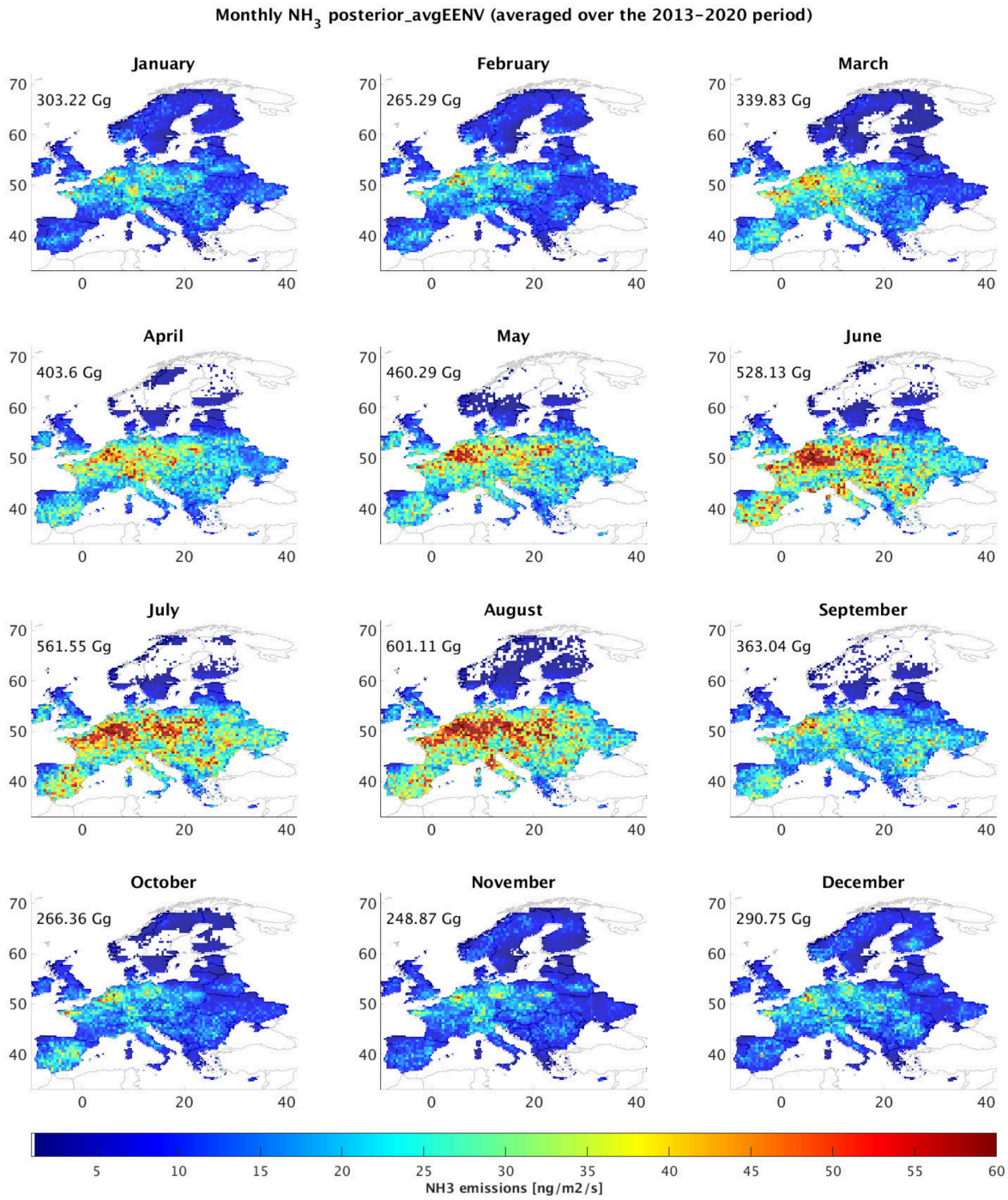

Supplementary Figure S 2. Spatial distribution of monthly posterior emissions of ammonia over Europe averaged over the eight-year period (2013–2020). Ammonia increases gradually from spring (March) when the fertilization period starts in Europe and peaks in August due to temperature dependent volatilization. After summer, when fertilization is forbidden, it rapidly declines with a minimum in November.

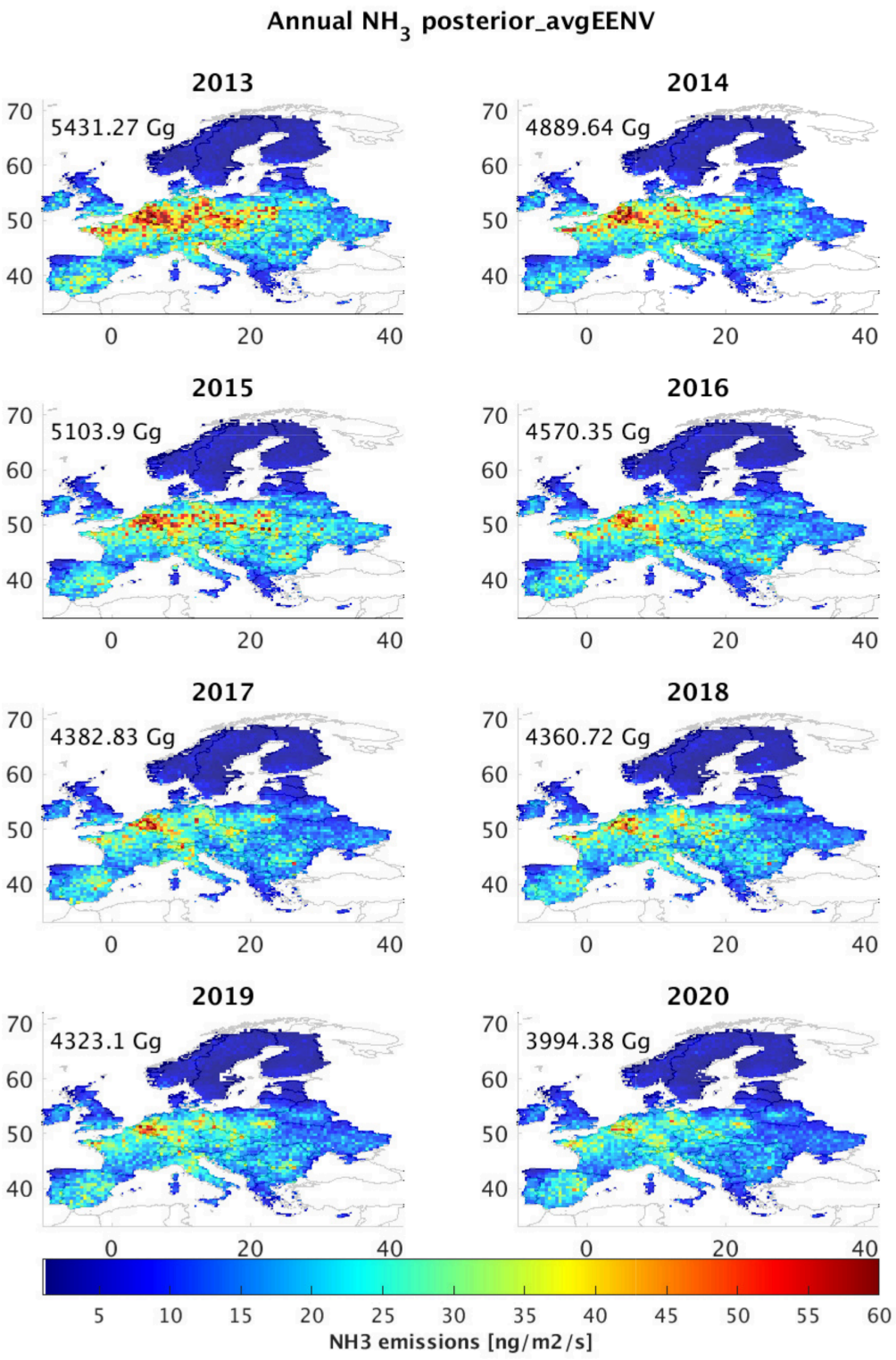

Supplementary Figure S 3. Spatial distribution of annual posterior emissions of ammonia over Europe during 2013–2020. Except for a small increase in 2015, emissions of ammonia decreased from 5431 Gg in 2013 to 3994 Gg in 2020.

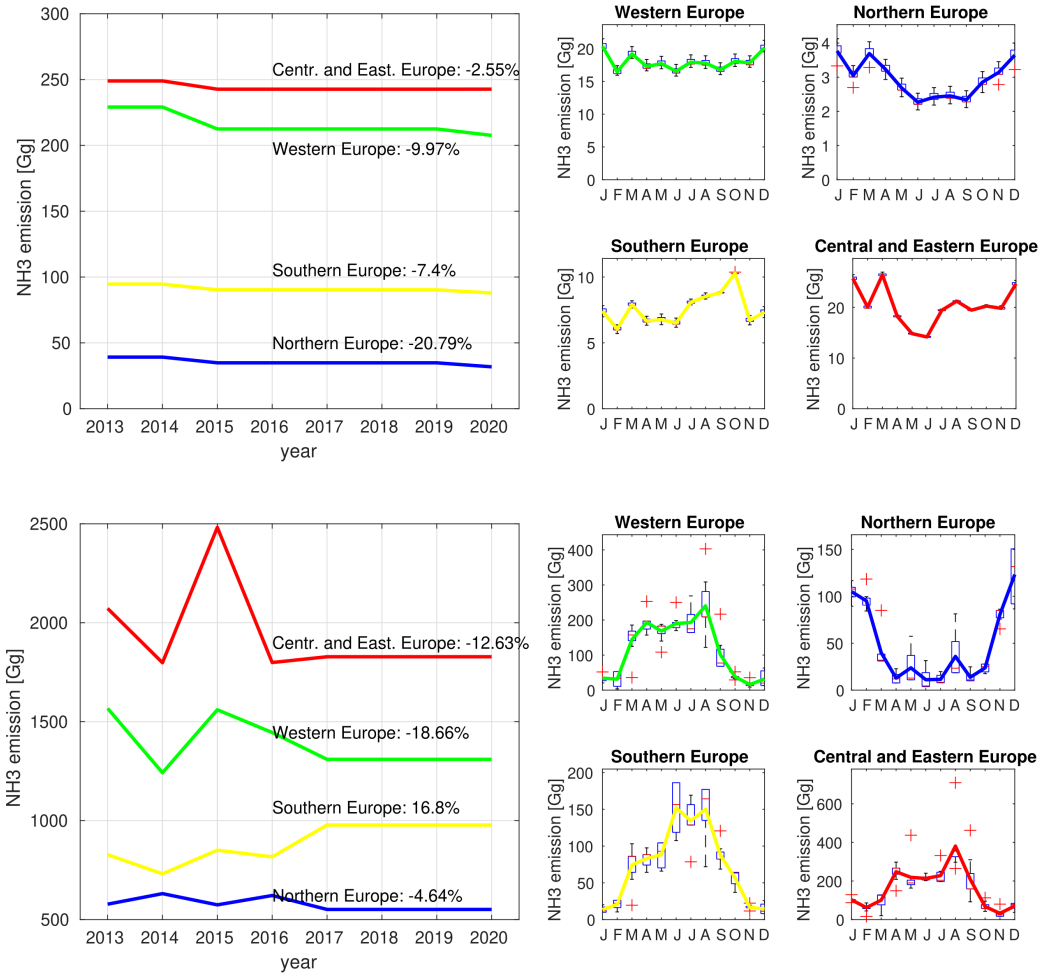

Supplementary Figure S 4. Left: Annual prior (EC6G4 and NE) emissions of ammonia in Southern (yellow), Western (green), Northern (blue), and Central and Eastern (red) Europe. Right: Monthly average prior (EC6G4 and NE) emissions of ammonia accompanied by box plots, where the red line indicates the median, the bottom and top edges of the box indicate the 25th and 75th percentiles, respectively, and the whiskers extend to the most extreme data points (not considered outliers), which are represented using red crosses.

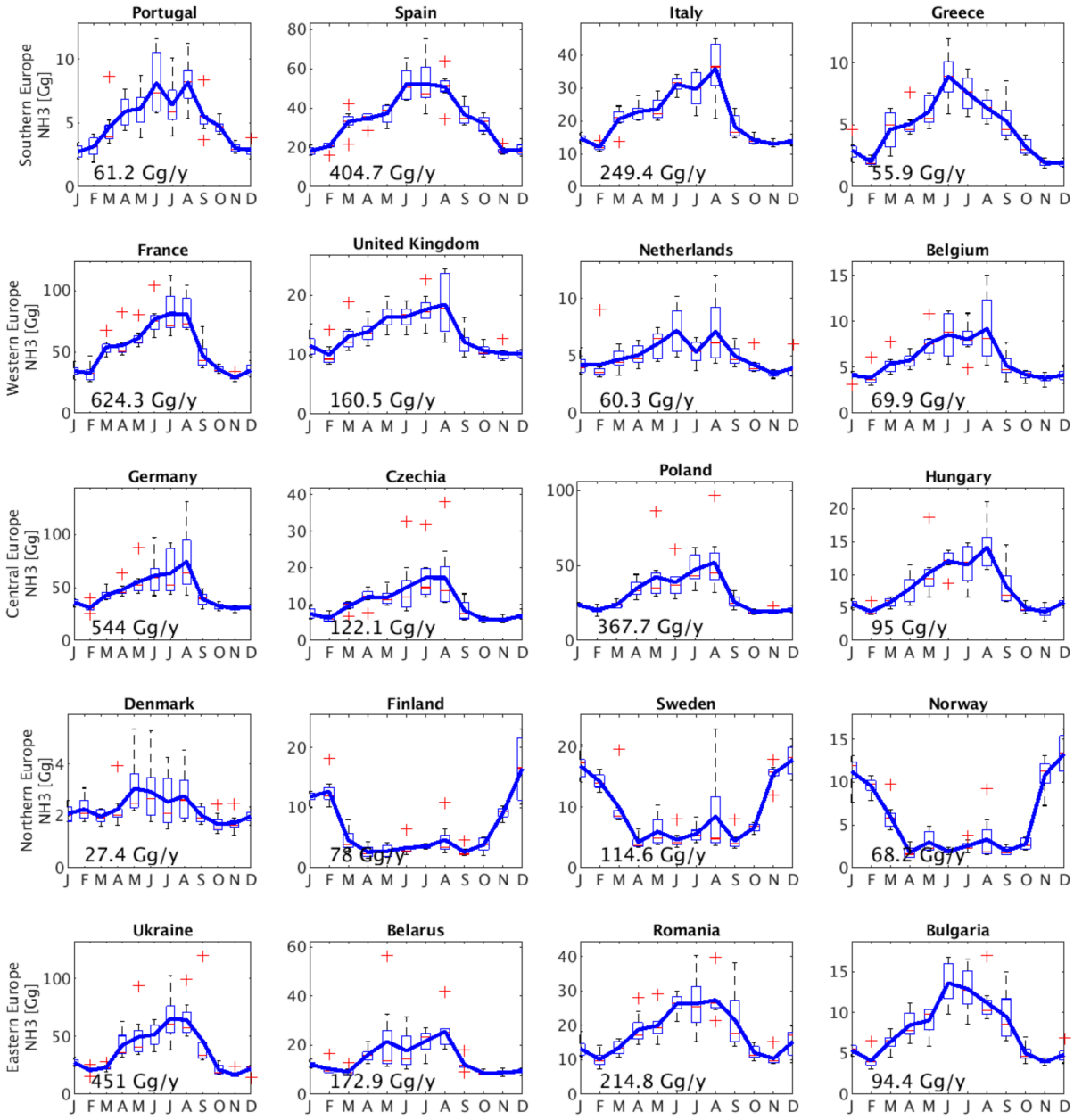

Supplementary Figure S 5. Monthly average posterior emissions of ammonia accompanied by box plots, where the red line indicates the median, the bottom and top edges of the box indicate the 25th and 75th percentiles, respectively, and the whiskers extend to the most extreme data points (not considered outliers), which are represented using red crosses.

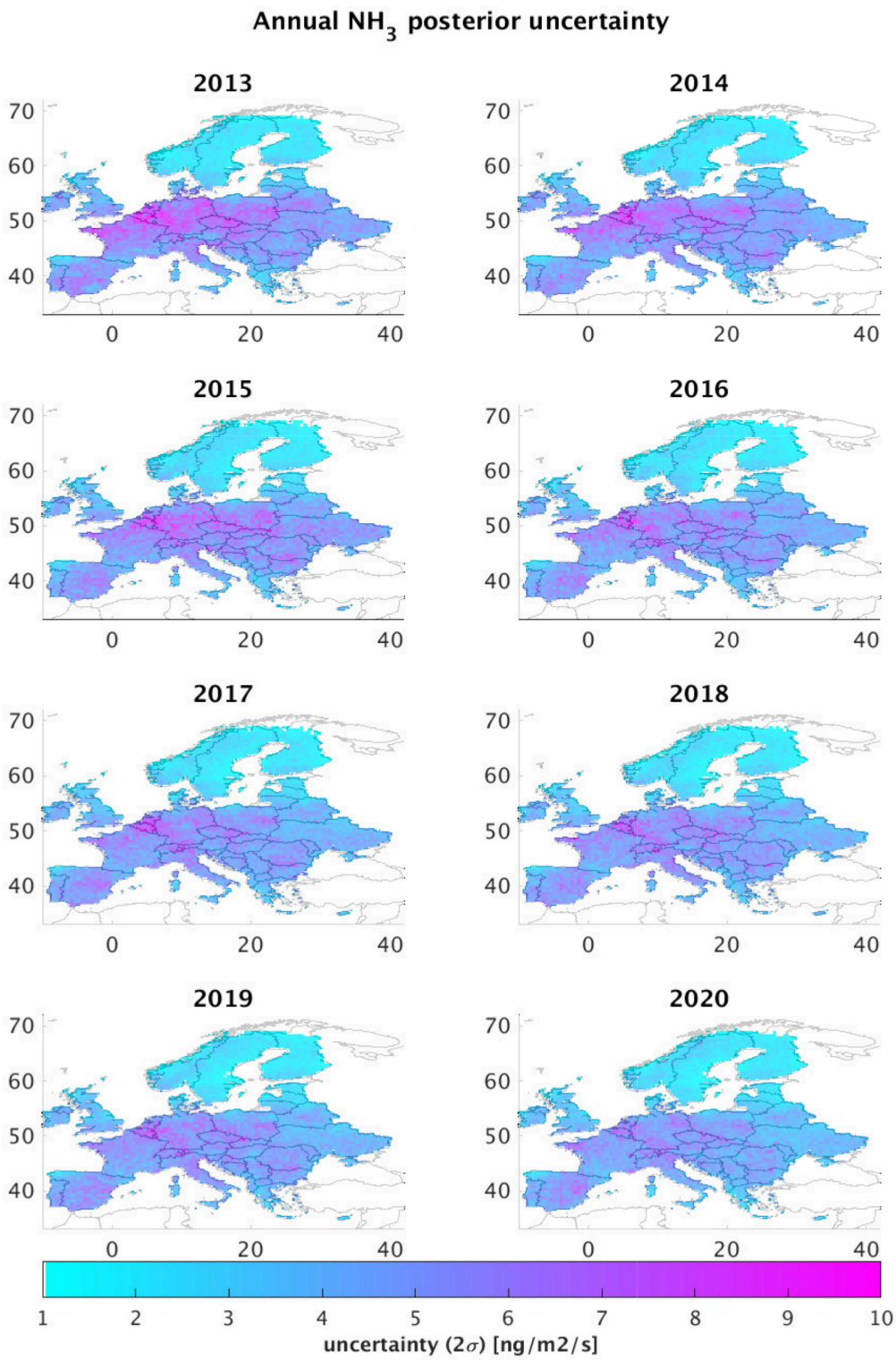

Supplementary Figure S 6. Absolute uncertainty of posterior emissions of ammonia calculated as 2 σ for each year of the study period 2013–2020.

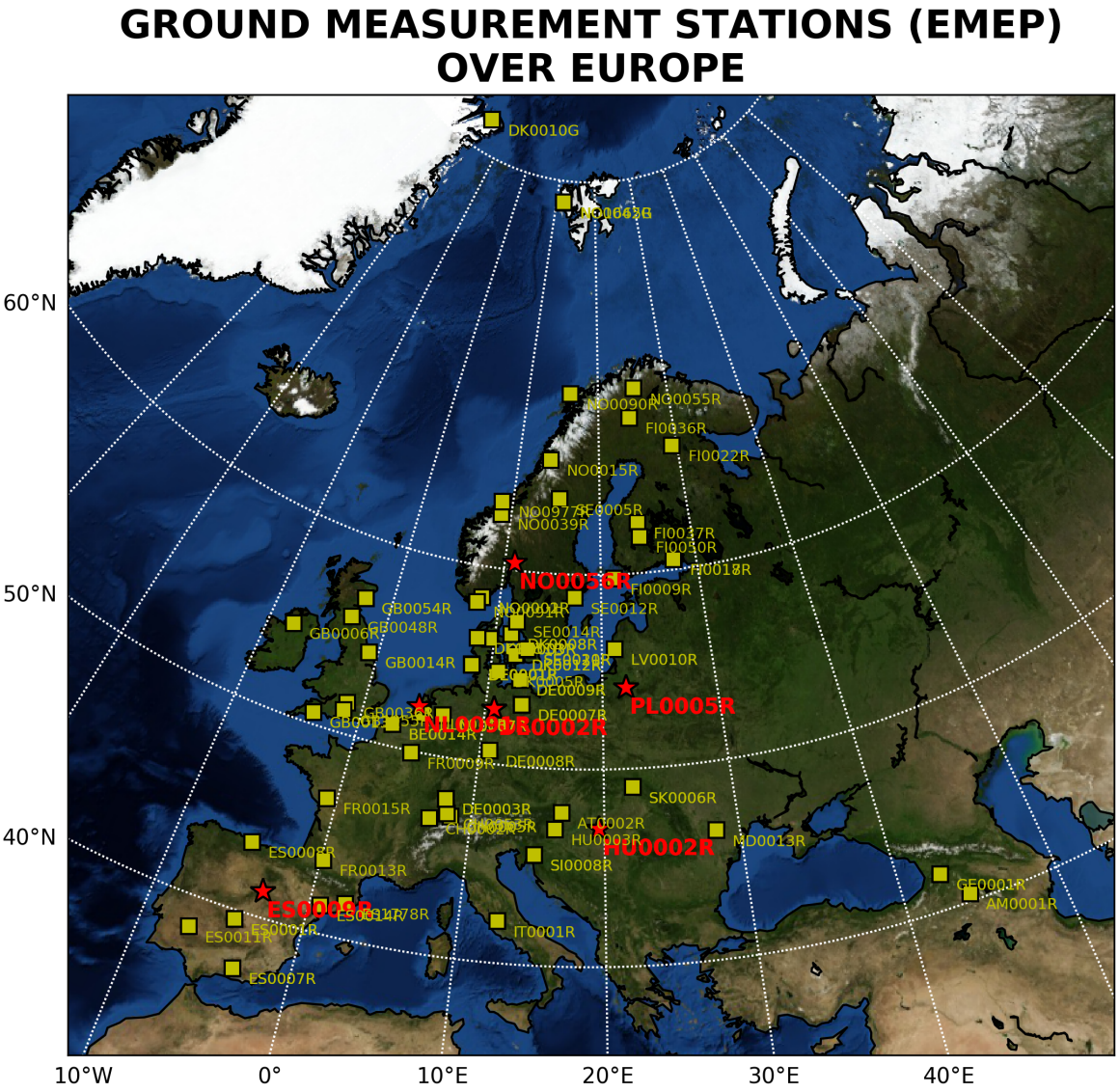

Supplementary Figure S 7. The EMEP (European Monitoring and Evaluation Programme, https://emep.int/mscw/) network, which consists of 53 stations over Europe. For each station we used a total of 2829 observations in our comparison that were averaged to the temporal resolution of our modelled concentrations (daily). The six stations highlighted with red color are random stations, for which a timeseries comparison was performed for v^{mod} using prior and posterior emissions against ground-based ammonia (see Supplementary Figure S 8).

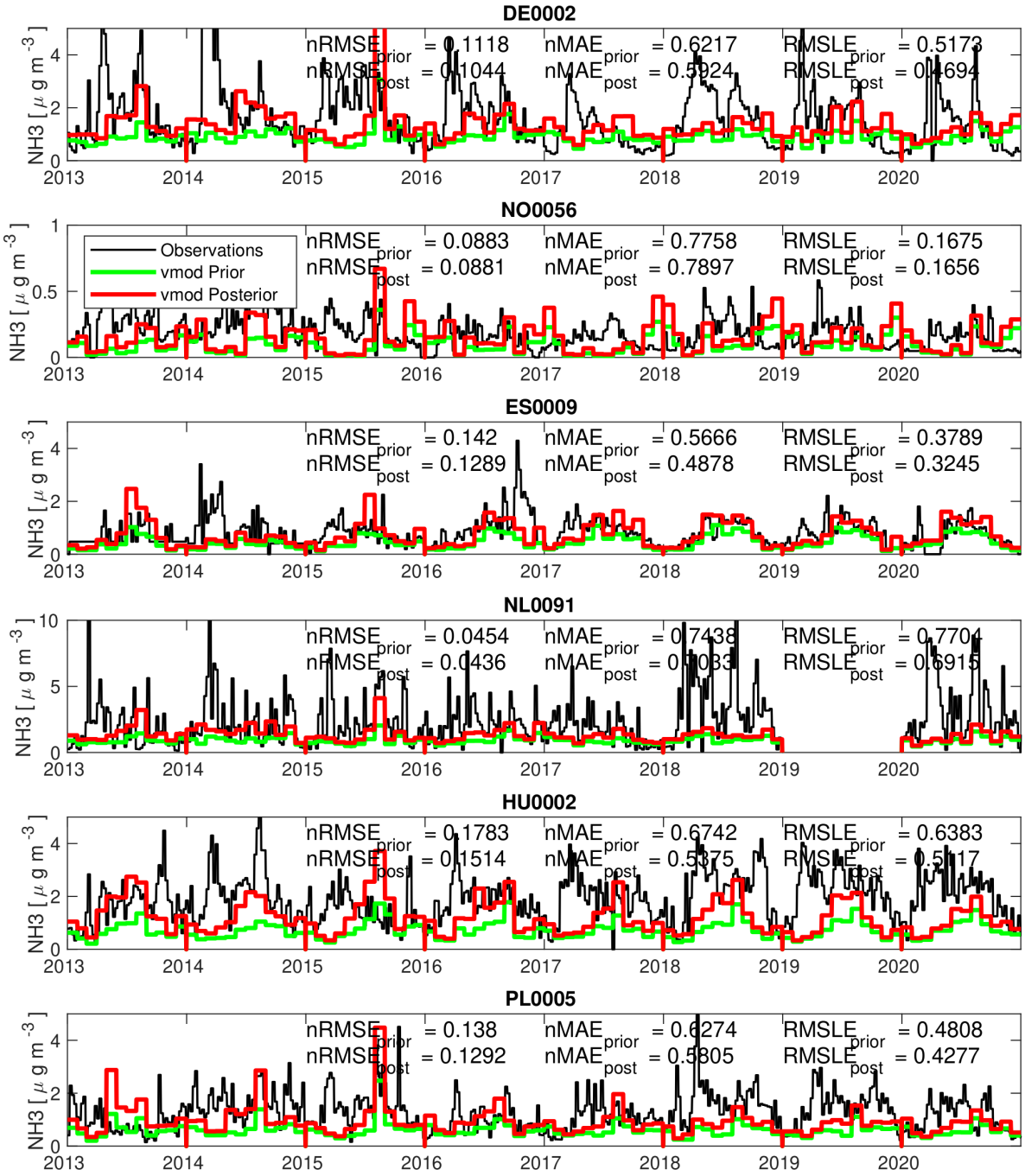

Supplementary Figure S 8. Timeseries of prior (green) and posterior (red) modelled surface ammonia concentrations over the whole study period (2013–2020) against ground-based observations from six EMEP stations (DE0002 in Germany, NO0056 in South Norway, ES0009 in Spain, NL0091 in the Netherlands, HU0002 in Hungary and PL0005 in Poland). For ease of visualization of the modelled and measured concentration and for smaller computational time, we averaged observations every week and modelled concentrations every month.

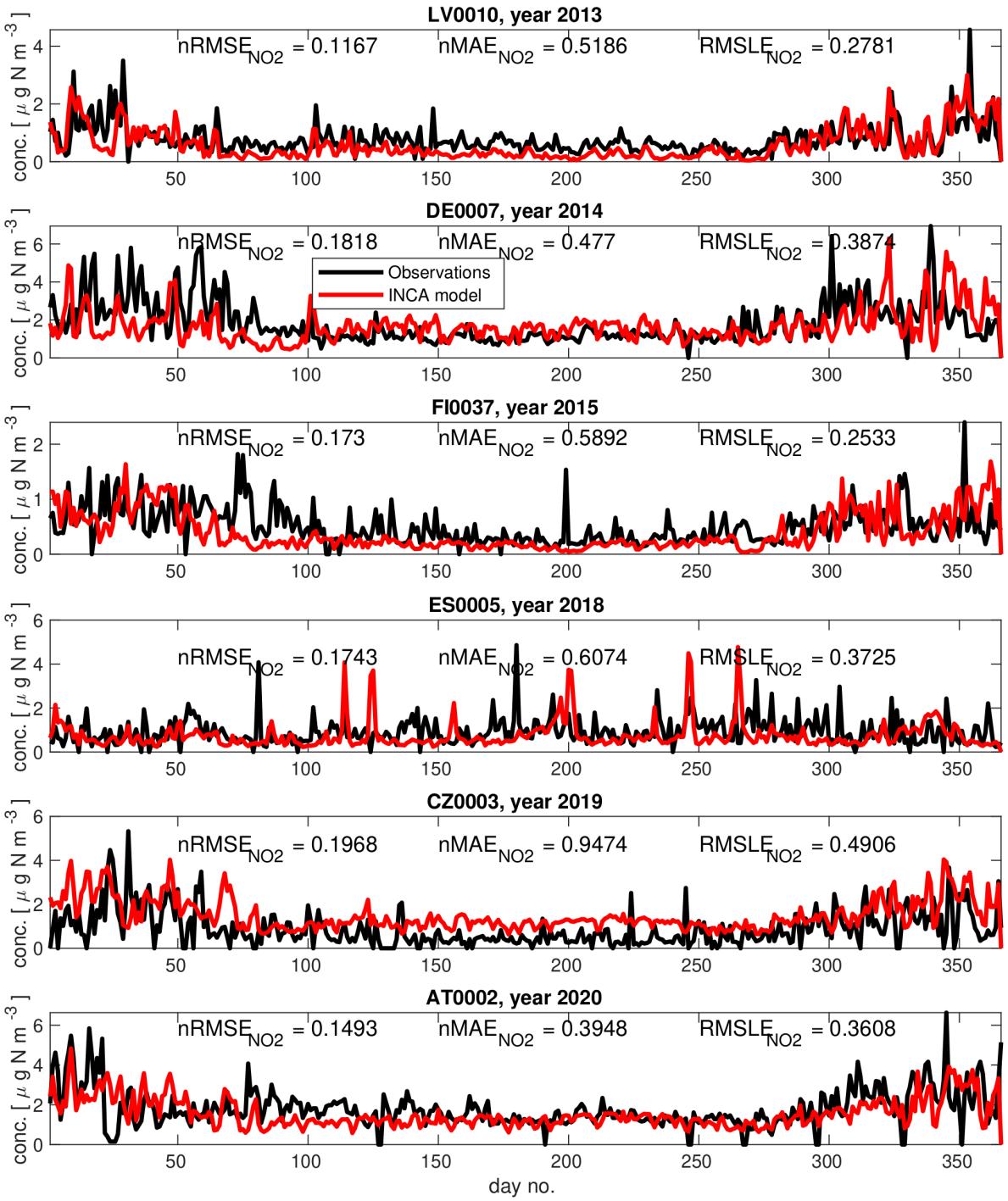

Supplementary Figure S 9. Timeseries of modelled surface NO2 and SO2 concentrations against ground-based observations. Six random EMEP stations for different years were processed for each species, namely LV0010 in Latvia, DE0007 in Germany, FI0037 in Finland, ES0005 in Spain, CZ0003 in Czechia and AT0002 in Austria for NO2 and NL0009 in the Netherlands, ES0012 in Spain, SE0012 in Sweden, LT0015 in Lithuania, FI0009 in Finland and ES0005 in Spain for SO2. Relevant statistics showing the model performance in the calculated NO2 and SO2 concentrations are also depicted.

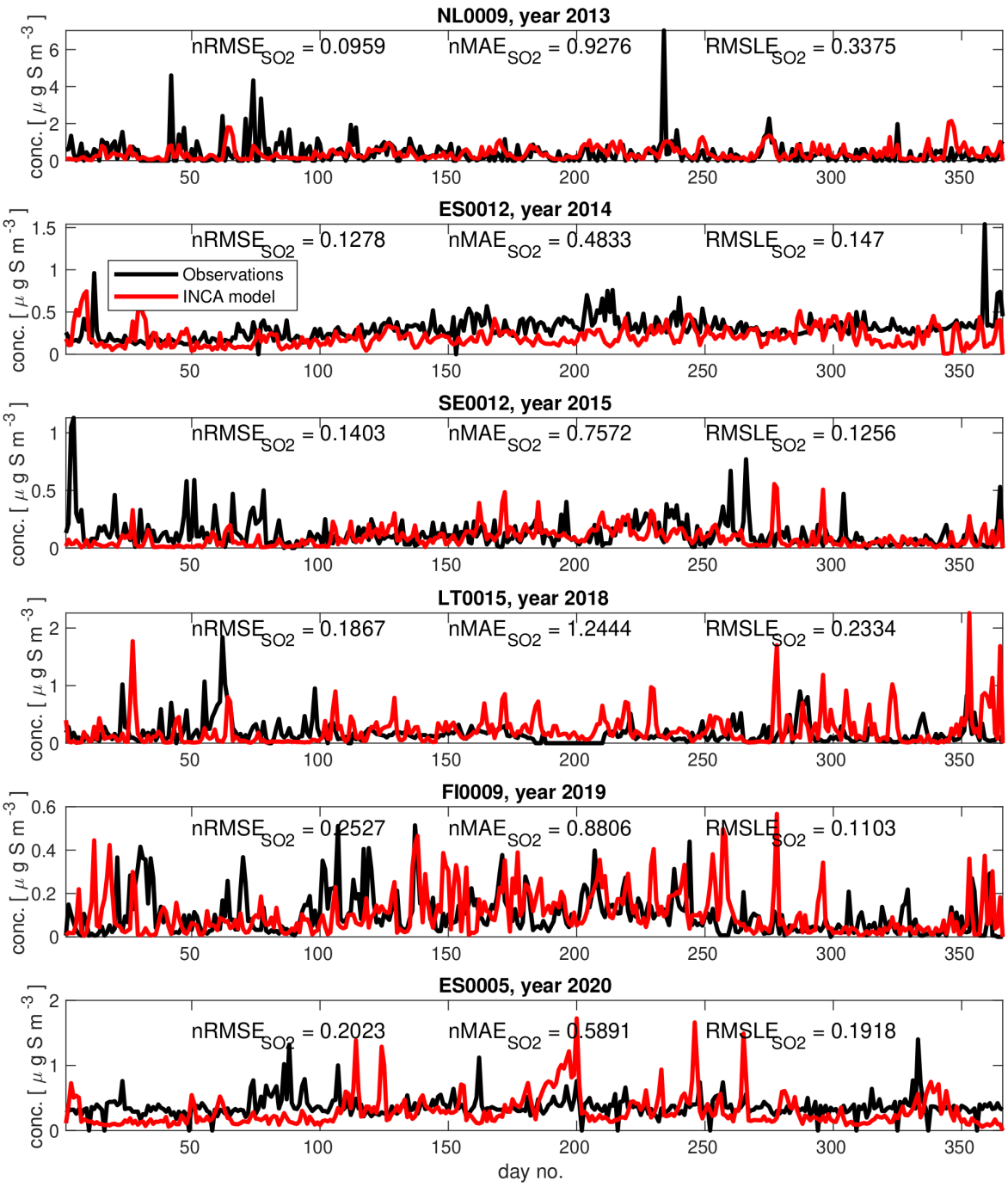

Supplementary Figure S 9. *Continued.*

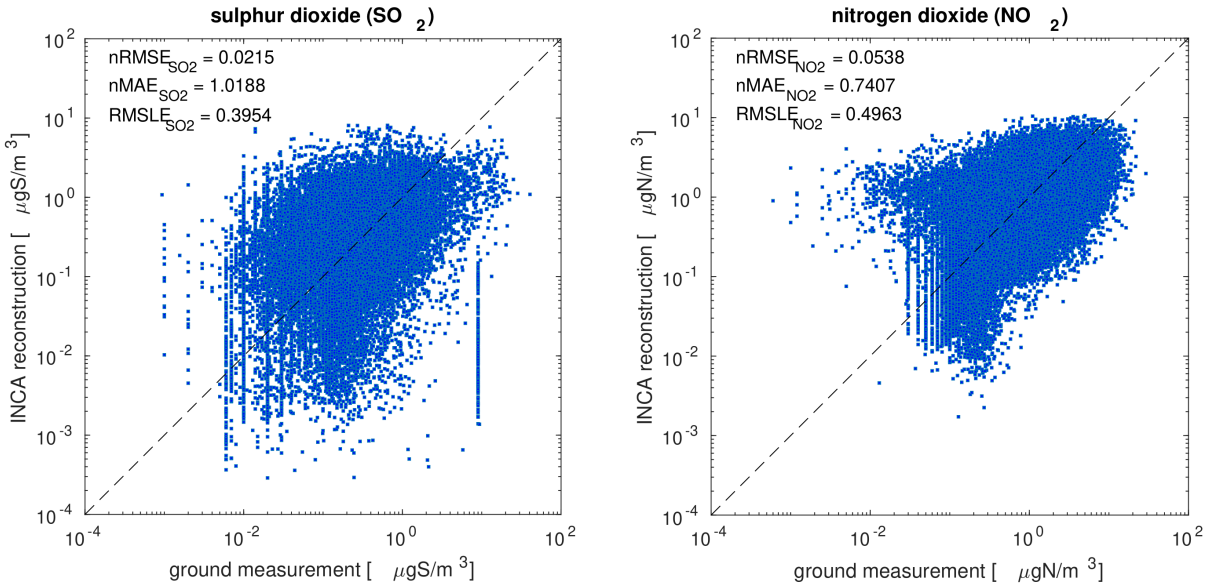

Supplementary Figure S 10. Scatterplot of modelled SO2 and NO2 surface concentrations against observations from 53 EMEP stations (https://emep.int/mscw/) from all over Europe for the period of our study. A total number of 3,368,660 for SO2 and 4,252,592 for NO2 was used for the evaluation of the model performance; relevant statistics are also calculated.

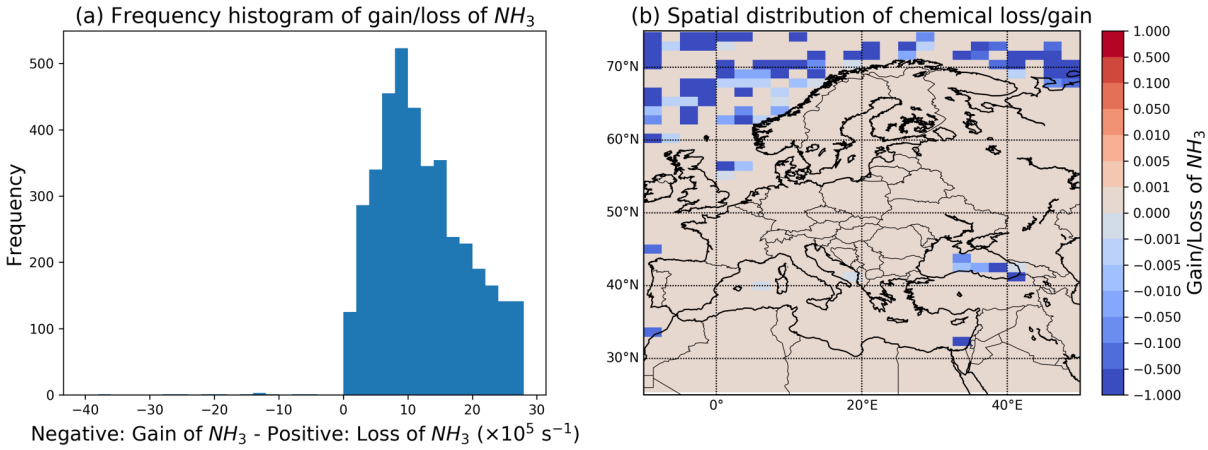

Supplementary Figure S 11. (a) Frequency distribution of gain (negative values) and loss of atmospheric ammonia in the inversion domain (10°W–50°E, 25°N–75°N) during the study period (2013 – 2020). Only the altitudes where satellite ammonia has an influence in the inversion were considered (~1018-619 hPa). The distribution shows that shift of the equilibrium reaction with nitric acid towards production of gaseous ammonia is a rather rare event and could be omitted. (b) Spatial projection of the occurrences of loss and gain of atmospheric ammonia in the inversion domain during the study period (2013 – 2020). Pixels where gain of atmospheric ammonia occurs are located in marine regions, for which ammonia emissions were not constrained.

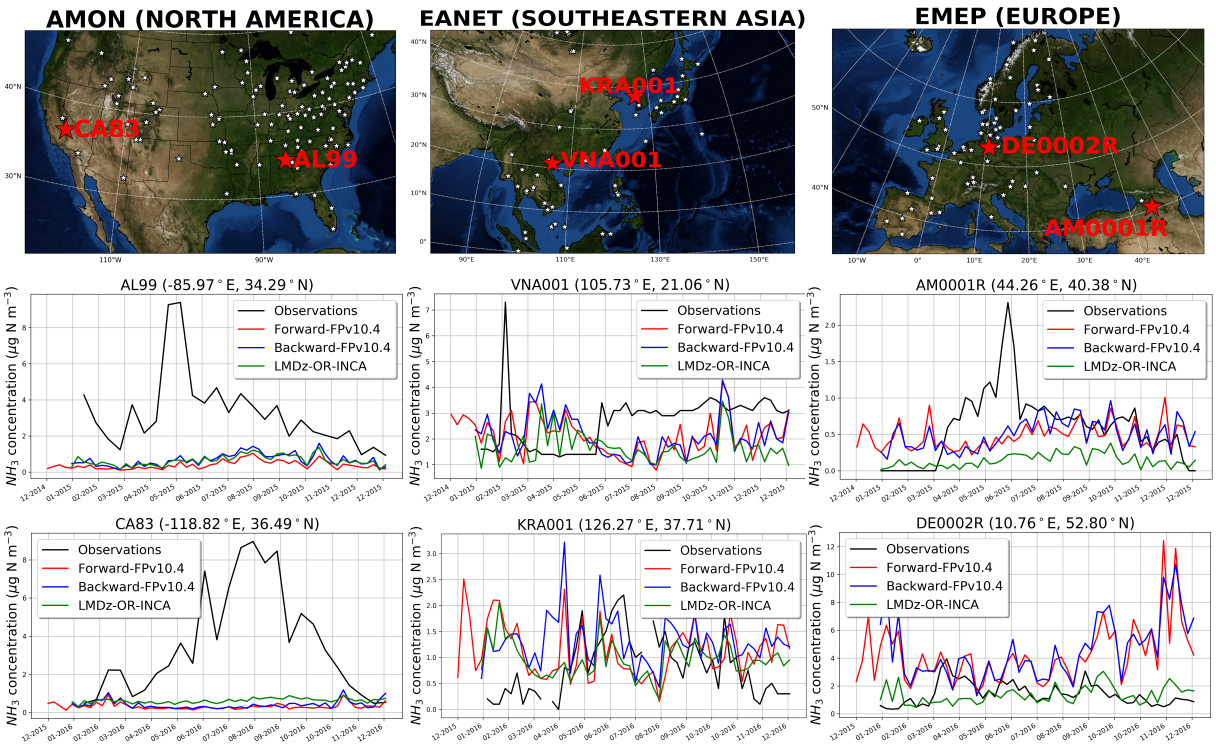

Supplementary Figure S 12. Locations and timeseries concentrations of nitrogen at stations from AMoN (North America, EANET (Southeastern Asia) and EMEP (Europe) networks used for validation. Forward and backward modelled concentrations of FLEXPART averaged for the temporal resolution of the observations are shown together with the respective concentrations from the Eulerian LMDz-OR-INCA using emissions from EGG (Bouwman et al., 1997; Giglio et al., 2013; Klimont et al., 2017). A very good agreement for all modelled concentrations is apparent that indicates the robust approach of our assumption that atmospheric ammonia is most often chemically depleted. The plot does not aim to show a model validation for the posterior ammonia against EMEP, but rather that model development to account for the chemical loss of ammonia produces reasonable results.

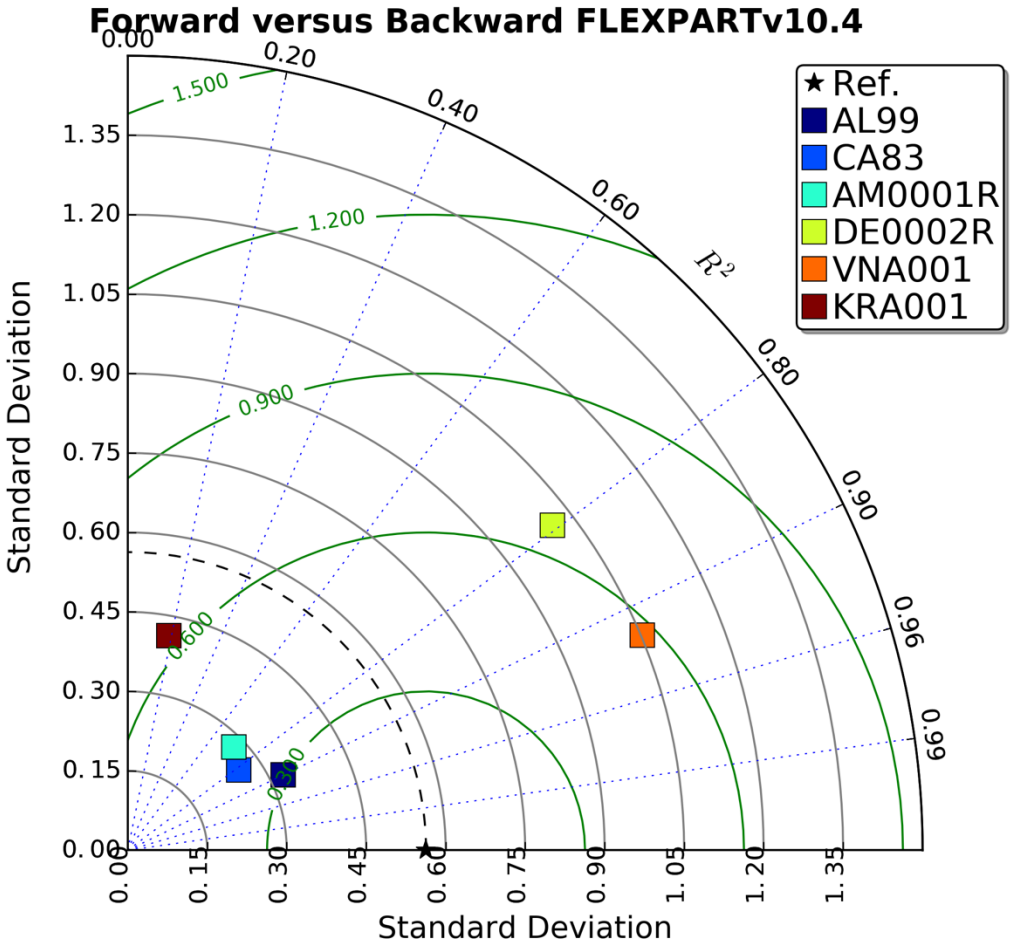

Supplementary Figure S 13. Taylor diagram of modelled concentrations of ammonia with FLEXPARTv10.4 in forward and backward mode using emissions from EGG (Bouwman et al., 1997; Giglio et al., 2013; Klimont et al., 2017). The diagram shows the Pearson's correlation coefficient (gauging similarity in pattern between the forward and backward simulated concentrations) that is related to the azimuthal angle (blue contours); the standard deviation of modelled concentrations is proportional to the radial distance from the origin (black contours) and the centered RMSE of modelled concentrations is proportional to the distance from the reference standard deviation (green contours). In most cases, forward and backward simulated concentrations are associated with Pearson's correlation coefficient above 0.7, and low standard deviations (<1 µg N m-3) and RMSEs (<0.7 µg N m-3), which implies the coherence of the two versions. The plot does not aim to show a model validation for the posterior ammonia against EMEP, but rather that model development to account for the chemical loss of ammonia produces reasonable results.